JOURNAL OF AIRCRAFT
Vol. 40, No. 6, November–December 2003

Transonic Cavity-Convex Corner Interactions

Kung-Ming Chung*
National Cheng-Kung University, Tainan 711, Taiwan, Republic of China

An experimental study was conducted to investigate the transonic convex-corner flows with and without the presence of an upstream cavity. Measurements were made to investigate the geometric effect and the spacing of a cavity on attached and separated convex-corner flows. The upstream expansion and downstream initial recompression are strongly affected by the upstream cavity, which includes the delay on the transition of subsonic and transonic expansion flows, the initial boundary-layer separation, the characteristics of separated flow, and the intensity of surface pressure fluctuations.

Nomenclature

C_p	=	pressure coefficient, $(p_w - p_\infty)/q_\infty$
$C_{\sigma p}$	=	pressure fluctuation coefficient, $(\sigma_p - \sigma_{p\infty})/q_\infty$
D, L	=	cavity depth and length
M_∞	=	freestream Mach number
p_w	=	static surface pressure
q_∞	=	dynamic pressure
X^*	=	x/δ
x	=	longitudinal coordinate
Z	=	distance between the cavity trailing edge and the corner
Z^*	=	Z/δ
δ	=	upstream undisturbed boundary-layer thickness
η	=	convex-corner angle, deg
ξ	=	separation length
σ_p	=	Surface pressure fluctuation

Introduction

DEFLECTED control surfaces can be used in combination to provide variable camber control during cruise flight.[1] A simplified upper deflected surface (convex-corner flow) was studied by Chung.[2] For subsonic expansion flows, the presence of the convex corner in a turbulent boundary layer results in strong upstream expansion and downstream recompression. The interaction region depends on freestream Mach number and the convex-corner angle. Transonic expansion flows result in milder initial recompression downstream of the corner, and the supersonic region may extend throughout the measurement location at higher $M_\infty^2\eta$. The flow is separated at $M_\infty^2\eta = 8.96$, and the peak interaction is observed at the location of separation. The measurements of surface pressure fluctuations indicate the intermittent nature of the pressure signal, and the amplitude of peak pressure fluctuations could be scaled with $M_\infty^2\eta$. The unsteadiness of the flows is related to the type of expansion flow and the shock wave excursion.

Furthermore, presence of a cavity in transonic flow results in a stronger expansion near the cavity trailing edge[3] and induces large vortical structure propagating downstream.[4] The upstream cavity, which may represent cutouts or gaps, upstream of a deflected control surface, would have a significant influence on its aerodynamic characteristics. Furthermore, the boundary-layer development upstream of the corner would have a strong influence on the criterion of initial separation. It is considered that the upstream cavity can be used for the passive control of the separated convex-corner flow, which includes the influence on the upstream expansion, the downstream recompression, and the recovery process. For the present study, the test configuration is shown in Fig. 1. A cavity is located at about one to three boundary-layer thicknesses upstream of the convex corner. The measurements of mean and fluctuating pressures downstream of the corner were conducted to investigate the cavity-convex corner interactions.

Received 19 November 2002; revision received 16 January 2003; accepted for publication 24 January 2003.

*Research Fellow, Aerospace Science and Technology Research Center, 2500 Section 1, Chung-Cheng South Road, Kueijen; kmchung@astrc.iaalab.ncku.edu.tw. Senior Member AIAA.

Experiment

Facility

The Aerospace Science and Technology Research Center/National Cheng-Kung University transonic wind tunnel is a blowdown type. The operating Mach number ranges from 0.2 to 1.4, and the simulated Reynolds number is up to 20×10^6/m. Major components of the facility include compressors, air dryers, cooling water system, storage tanks, and the tunnel. The dew point of high-pressure air through the dryers is maintained at -40°C under normal operation conditions. Air storage tank volume is 180 m^3 at 5.15 MPa. The test section is 600 mm square and 1500 mm long. In the present study, the test section is assembled with solid sidewalls and perforated top/bottom walls to reduce the amplitude of background acoustic waves.

For the data acquisition system, the NEFF Instruments System 620 and the LeCroy waveform recorders were used. The test conditions were recorded by the NEFF system while the LeCroy 6810 waveform recorders were used for the surface pressure measurements. A host computer with CATALYST software controls the setup of LeCroy waveform recorders through a LeCroy 8901A interface. All input channels were triggered simultaneously by using an input channel as the trigger source. The output range of waveform recorders was adjusted with an optimum resolution, and the relative error of the mean pressure signals is estimated to be about 0.1%.

Test Models

The test model consists of a flat plate, an interchangeable plate with a cavity, and the instrumentation plate. It is supported by a single sting, which is mounted on the bottom wall of the test section. The boundary layer is developed naturally along the flat plate, and the trailing edge of the cavity is located at about one to three boundary-layer thicknesses upstream of the convex corner. The length-to-depth ratio L/D of the cavities is from 2.0 to 35.0, and the width is 60 mm for all of the test cases. Three instrumentation plates, with 13-, 15-, and 17 ± 0.1-deg convex-corner angle, were fabricated. One row of 10 holes, 6 mm apart and 2.5 mm in diameter, along the centerline of each instrumentation plate was drilled perpendicularly to the test surface.

All of the pressure transducers within the holes were flush mounted to the test surface and potted using silicone rubber sealant. Flushness of the pressure transducers was checked by a machinist's block to minimize the interference with the flow. The side fences at both sides of the instrumentation plate were installed to prevent crossflow.

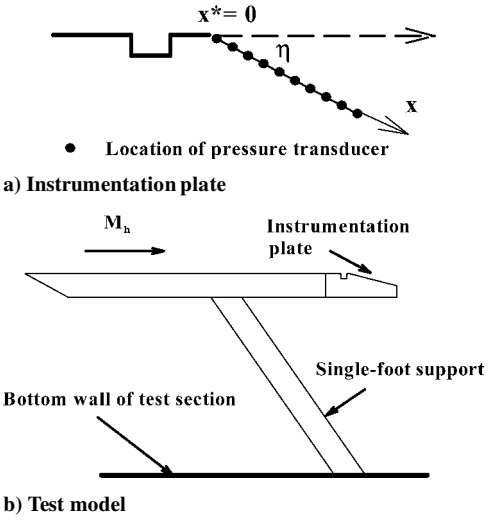

Fig. 1 Test configuration.

Experimental Techniques

For the surface pressure measurements, Kulite (Model XCS-093-25A, B screen) pressure transducers were used. The outside diameter is 2.36 mm, and the sensing element is 0.97 mm in diameter. The natural frequency is 200 kHz as quoted by the manufacturer. The pressure transducers are powered by a TES Model 6102 power supply at 15.0 V. In addition, external amplifiers (Ecreon Model E713) were used. With a gain of 20, the rolloff frequency is about 140 kHz. Note that there is high-frequency damping due to the transducer's size. Corcos's criterion[5] indicates that the maximum measurable frequency of a given pressure transducer, $f_{\max}$, is approximately equal to $U_c/2\pi r$, where r is the radius of the pressure transducer and U_c is the convection velocity. Under the present test condition, $f_{\max} \approx 55$ and 70 kHz for $M_\infty = 0.64$ and 0.83, respectively. The sampling period is 5 μs (200 kHz). Furthermore, the uncertainty of the experimental data based on the flat plate case is estimated to be 0.43 and 0.15% for the static pressure coefficient and surface pressure fluctuation coefficient, respectively.[2]

The oil-flow visualization technique is used to check the two dimensionality of the flow and to visualize the surface flow pattern. A thin film of the mixture (titanium dioxide, oil, oleic acid, and kerosene) is applied on the surface of the instrumentation plate. The region of separation was visualized and compared with the surface pressure measurements.

For the experiment, the test Mach number M_∞ is 0.64 and 0.83 ± 0.01. The stagnation pressure p_0 and temperature T_0 are 172 ± 0.5 kPa and room temperature, respectively. Undisturbed boundary-layer surveys were conducted at $x_{\text{le}} = 475$ mm (or 25 mm upstream of the convex corner). The normalized velocity profiles appear to be full ($n \approx 7$–11 for the velocity power law). Moreover, the study by Miau et al.[6] showed that the transition of the boundary layer under the present test condition is close to the leading edge of the flat plate. This indicates turbulent flow at the measurement locations. The boundary-layer thickness is 7.3 and 7.1 ± 0.2 mm, and the Reynolds number Re_{δ_0} is about 14.9 and 16.8×10^4 for $M_\infty = 0.64$ and 0.83, respectively.

Results and Discussions

Oil-Flow Pattern

For the convex-corner flow without an upstream cavity, the study of Chung[2] indicated that the limited size of the test model has a minor influence on the surface oil-flow pattern near the centerline region of the corner surface. It was also found that the convex-corner flow is separated at $M_\infty = 0.83$ and $\eta = 13$ deg. The separation bubble grows in both the upstream and downstream directions with increasing convex-corner angle, and the separation position moves slightly upstream, and the reattachment position moves downstream. With an upstream cavity, the limited width of the cavity shows some edge effect on the surface oil-flow pattern. However, the effect is considered to be negligible for the present study. Furthermore, all

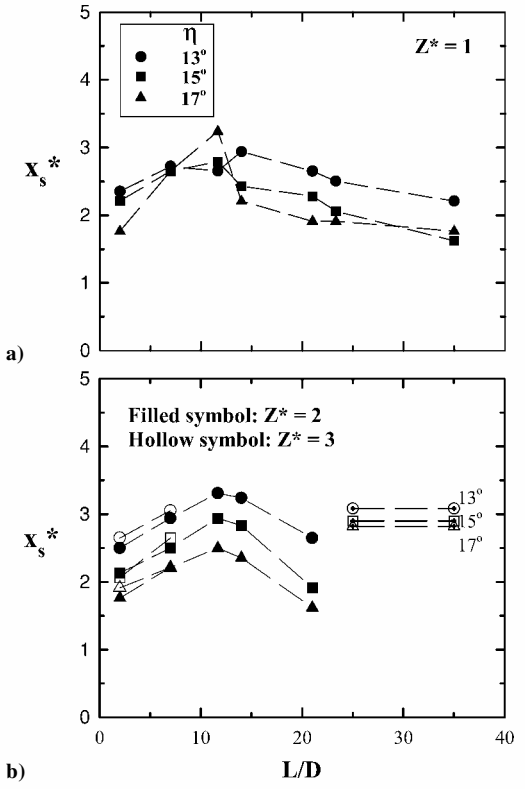

Fig. 2 Shock location.

test cases at $M_\infty = 0.64$ correspond to attached subsonic flow. The streamlines near the centerline region are straight and parallel to the incoming flow direction. At $M_\infty = 0.83$ and $\eta = 13$ deg, accumulation of titanium dioxide is observed at $X^* \approx 2.20 \sim 2.94$. This is due to the shock-induced adverse pressure gradient, and is taken as the shock or boundary-layer separation location X_s. Farther downstream, it was found that the deflection of streamlines is visible for $L/D = 23.3$ and 35.0 (shallow cavity) at $Z^* = 1$. The end of streamline deflection is observed at $X^* \approx 4.62 \sim 6.32$, which is taken as the reattachment location. For $L/D \leq 21.0$, the deflection of the streamline is hardly to be seen. This indicates that the presence of an upstream deeper cavity delays the initial boundary-layer separation of transonic convex-corner flow. As the cavity moves away from the convex corner ($Z^* = 2$), the deflection of streamlines is not visible for $L/D \leq 7.0$. It is clear that the upstream cavity effect on the delay of initial boundary-layer separation is degraded. For $Z^* = 3$, the separation of boundary layer is observed for the both test cases ($L/D = 2.0$ and 7.0).

Observation of the shock location at $M_\infty = 0.83$ is summarized in Fig. 2. The cases of transonic convex-corner flow without an upstream cavity are also shown for reference (Fig. 2b). At $Z^* = 1$ (Fig. 2a), presence of the transitional-type cavities ($L/D \approx 11.7$–14.0) shows a minor effect on the shock location while the shock wave moves upstream (or decreasing X_s^*) with decreasing or increasing L/D (closed- or open-type cavities), particularly for $\eta = 15$ and 17 deg. This implies a more extensively separated region. At $Z^* = 2$, the variations of shock location with L/D show similar trends as the cases at $Z^* = 1$. However, the shock wave for $\eta = 13$ deg moves slightly downstream (or increasing X_s^*) with the transitional-type cavity ($L/D \approx 11.7$–14.0). For $\eta = 15$ and 17 deg, the upstream movement of shock wave is more evident than in the cases at $Z^* = 1$. This is considered to be due to the cavity effect on the initial expansion process upstream of the corner. Note that the influence of the relative distance between the cavity trailing edge and the corner ($Z^* = 2$ and 3) on the shock location is not significant at $L/D = 2.0$ and 7.0 (Fig. 2b).

For $M_\infty = 0.83$ and $\eta = 13$ deg, the reattachment location for the convex-corner flow is located at $X_R^* \approx 7.93$ (Fig. 3). With the upstream cavity, the initial boundary-layer separation is delayed. Observation of the reattachment phenomena is only for $L/D \geq 23.3$

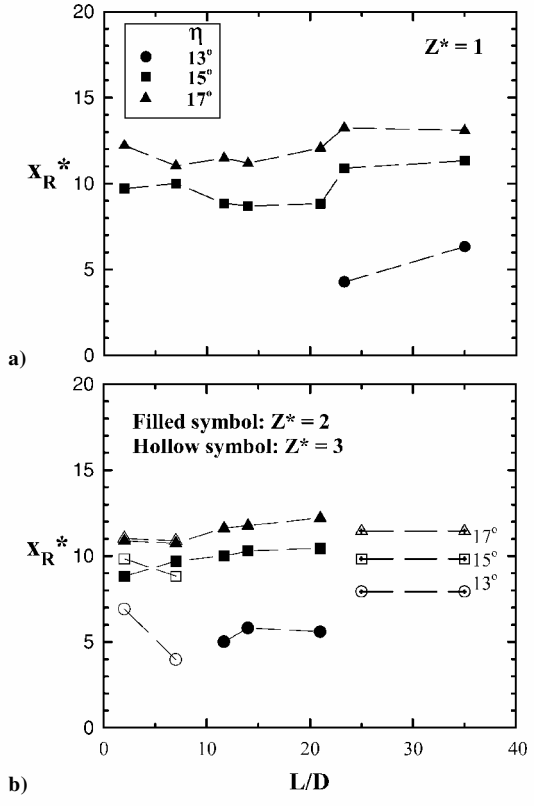

Fig. 3 Reattachment location.

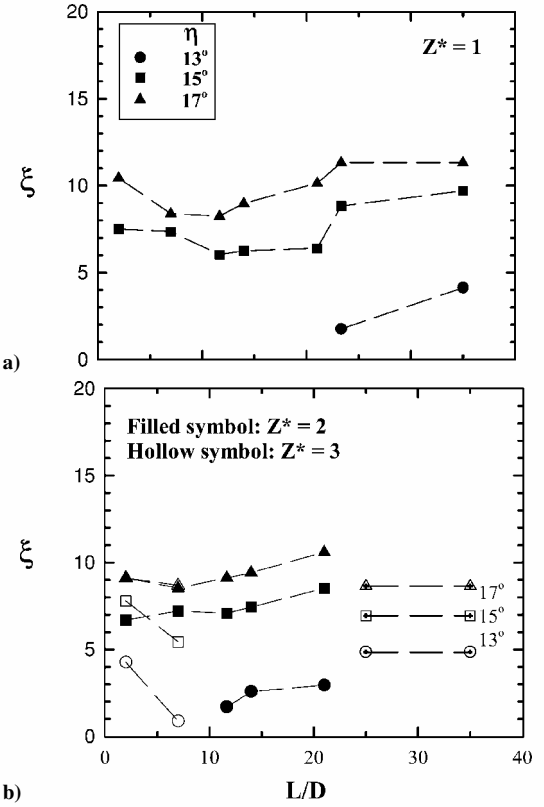

Fig. 4 Separated region.

at $Z^* = 1$, for $L/D \geq 11.7$ at $Z^* = 2$, and for $L/D \geq 2.0$ at $Z^* = 3$. In addition, Fig. 3 shows that the cavity results in upstream movement of the reattachment location, where $X_R^* \approx 3.97.0$–6.91. For $\eta = 15$ and 17 deg, variations of X_R^* show a similar trend. The reattachment location moves slightly downstream for $L/D \geq 23.3$ at $Z^* = 1$. At $Z^* = 2$ and 3, the cavity effect on X_R^* is minimized. Moreover, the separation length $\xi (= X_R^* - X_S^*)$, which is defined as the distance between the separation and reattachment positions, is summarized in Fig. 4. For $\eta = 13$ deg, it is found that the separation region decreases for all of the separated cases ($Z^* = 1$, 2, and 3). This implies that the upstream cavity may be used as passive control for the initial boundary-layer separation of transonic convex-corner flows. For the separated flows ($\eta = 15$ and 17 deg), the influence of the transitional-type cavities is minimized. However, the shallow cavities (closed-type cavities) result in the growth of separation bubbles, which correspond to the upstream movement of shock wave and slightly downstream movement of reattachment location. Note that the effect of Z^* is not significant.

Mean Surface Pressure Distributions

Examples of static pressure distribution along the centerline of the instrumentation plates for the subsonic expansion flow ($M_\infty = 0.64$ and $\eta = 13$ deg) are shown in Fig. 5a. The origin of the x coordinate is at the corner. Figure 5 shows an upstream expansion and a downstream compression. With an upstream cavity at $Z^* = 1$, the flow remains at the subsonic condition for all of the test cases. However, lower levels of static pressure are observed downstream of the corner. This corresponds to stronger expansion near the corner. The initial recompression also increases, particularly with decreasing L/D (or deeper cavity). At a farther downstream location, the flow is further compressed. The geometric effect of the cavity has a minor influence on the level of the downstream static pressure. Note that the downstream compressions ($\mathrm{d}p/\mathrm{d}x$) are roughly the same with and without an upstream cavity. For the transonic convex-corner flow ($M_\infty = 0.83$ and $\eta = 17$ deg), the flow is expanded to supersonic speed and is separated downstream of the corner (Fig. 5b). The cavity effect is limited near the corner. Higher levels of static pressure are observed immediately downstream of the corner, particularly for the closed-type cavities. The increase of static pressure is due to the

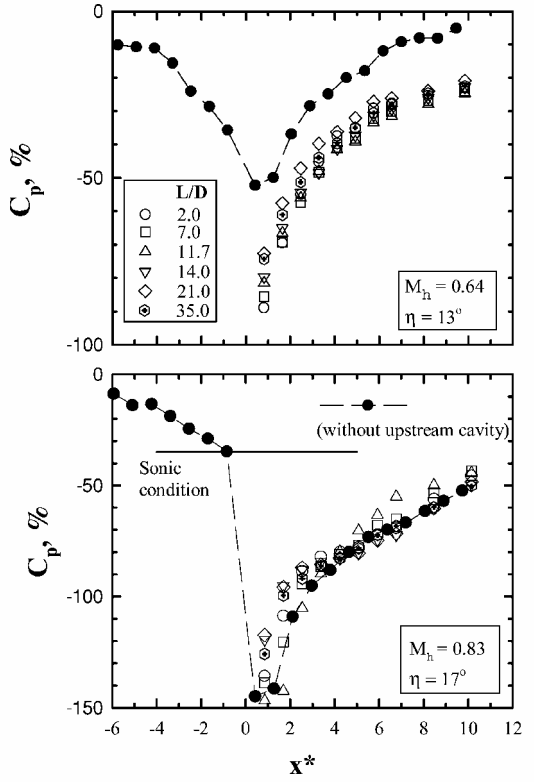

Fig. 5 Pressure distributions, $Z^* = 1$.

upstream movement of shock wave, which is also observed with the oil-flow visualization.

The minimum static pressure $C_{p,\min}$ near the corner is related to the upstream expansion and initial downstream compression process for the convex-corner flows. The study of Chung[2] indicates that the $C_{p,\min}$ values can be scaled with the parameter $M_\infty^2 \eta$. Stronger expansion is associated with increasing $M_\infty^2 \eta$ for the convex-corner flow, which also indicates higher peak Mach number near the corner.

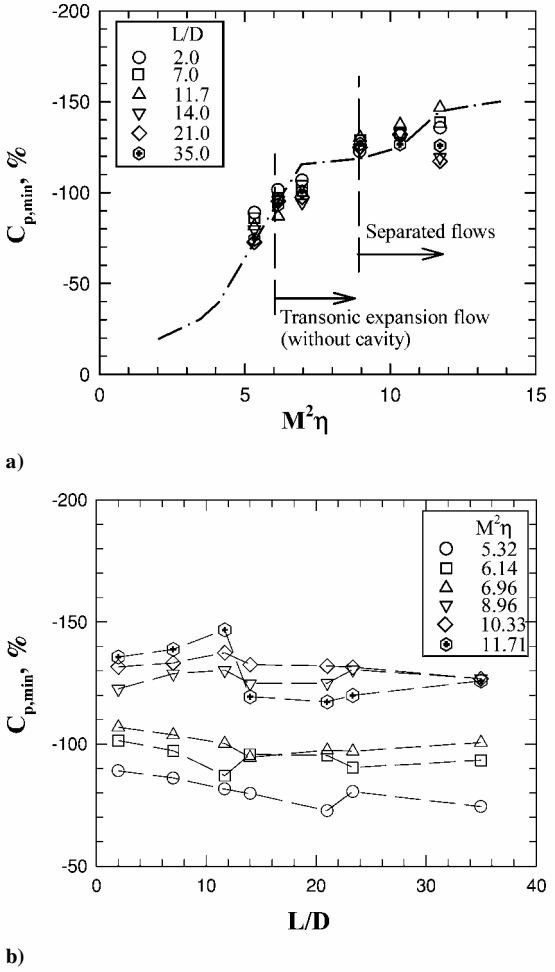

Fig. 6 Downstream expansion, $Z^* = 1$.

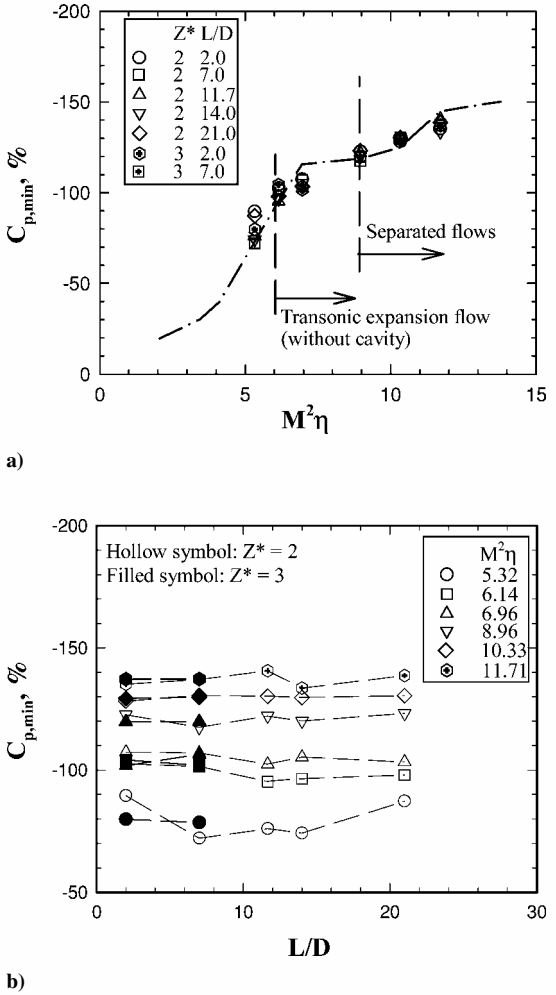

Fig. 7 Downstream expansion, $Z^* = 2$ and 3.

With the upstream cavities at $Z^* = 1$, the variations of the $C_{p,\min}$ value show a similar trend with and without the upstream cavity (Fig. 6a). However, it can be seen that the upstream cavity results in stronger expansion for the subsonic expansion flows ($M_\infty^2\eta = 5.33$). This could be due to the cavity effect on the development of upstream boundary layer. Less expansion for the separated flows ($M_\infty^2\eta = 11.71$) is also observed, particularly with the closed-type cavities. To further understand the geometric effect of the cavity on the minimum static pressure near the corner, the data are replotted in Fig. 6b. For the attached convex-corner flows ($M_\infty^2\eta \leq 6.96$) with open- or transitional-type cavities, the $C_{p,\min}$ values increase slightly with increasing L/D. This implies the delay on the transition of subsonic and transonic convex-corner flows. For the separated convex-corner flows ($M_\infty^2\eta \geq 8.96$), the $C_{p,\min}$ values decrease (stronger expansion) with the L/D up to 11.7. An increase is observed at $L/D = 14.0$, particularly for $M_\infty^2\eta = 11.71$. When the cavity moves away from the corner ($Z^* = 2$ and 3), the minimum static pressures are shown in Fig. 7. It can be seen that the cavity effect is degraded with increasing Z^* (Fig. 7a). There are only slight variations for the $C_{p,\min}$ values with and without the upstream cavity. Figure 7b shows that the L/D effect on $C_{p,\min}$ values for a given $M_\infty^2\eta$ is minimized, except for $M_\infty^2\eta = 5.32$ and $Z^* = 2$. This shows that the geometric effect of the cavity is more significant for the subsonic convex-corner flows.

Surface Pressure Fluctuations

To further understand the cavity effect on the convex-corner flows, examples of surface pressure fluctuation distributions are shown in Fig. 8. For the subsonic expansion flow ($M_\infty = 0.64$ and $\eta = 13$ deg), the pressure fluctuations C_{σ_p} increase upstream of the convex corner and reach the maximum immediately downstream of the corner followed by a sharp decrease. The rise of C_{σ_p} corresponds to the initial compression (or adverse pressure gradient) downstream of

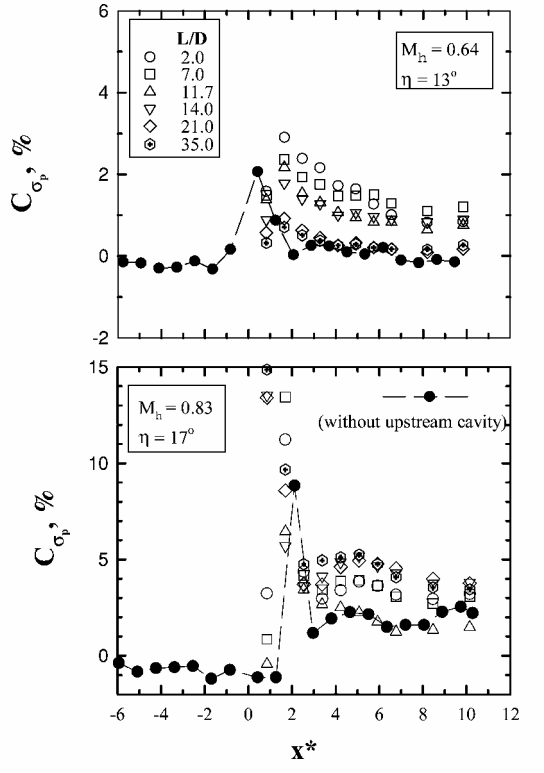

Fig. 8 Pressure fluctuation distributions, $Z^* = 1$.

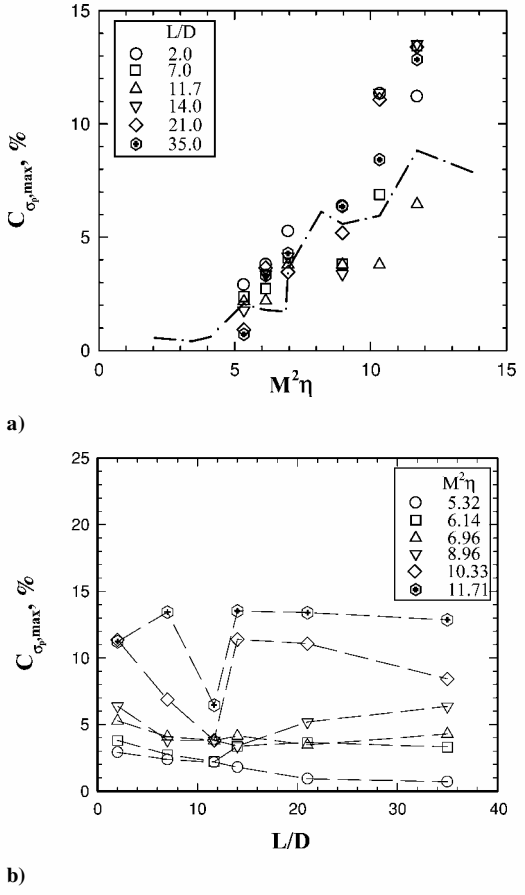

Fig. 9 Peak pressure fluctuations, $Z^* = 1$.

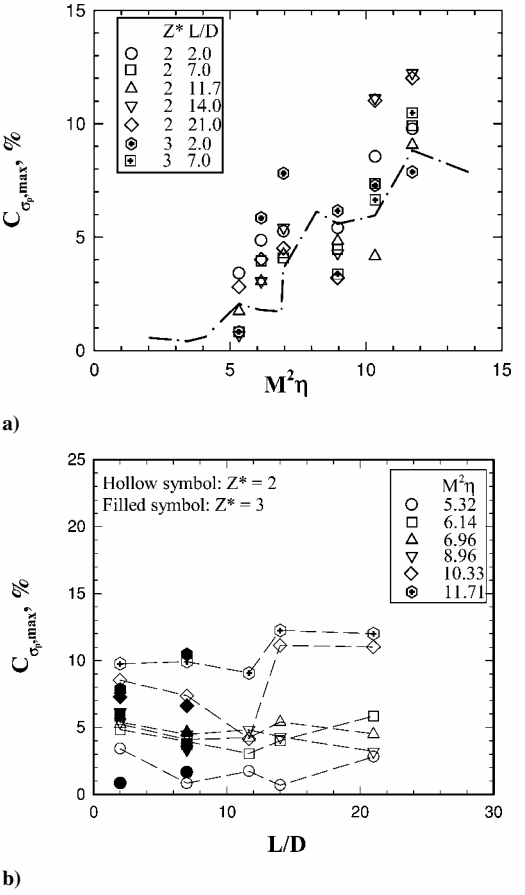

Fig. 10 Peak pressure fluctuations, $Z^* = 2$ and 3.

the corner. With the upstream cavity at $Z^* = 1$, lower levels of C_{σ_p} are observed at $X^* = 0.82$ (Fig. 8a). This is considered to be due to the stronger upstream expansion, as shown in the mean surface pressure distributions. The peak pressure fluctuations, which decrease with increasing L/D, are detected at a farther downstream location ($X^* = 1.64$) followed by a gradual decrease. The approximately equilibrium levels of pressure fluctuation at the farther downstream location ($X^* > 6.0$) with open- or transitional-type cavities ($L/D \leq 14.0$) are higher than the convex-corner flow without an upstream cavity. For the separated flow [$M_\infty = 0.83$ and $\eta = 17$ deg (Fig. 8b)], the characteristics of pressure fluctuation distributions are roughly the same with and without the upstream cavity. However, note that the peak pressure fluctuations are related to the L/D of the cavity, in which the peak pressure fluctuations are observed at $X^* = 1.69$ for $L/D \leq 11.7$ and at $X^* = 0.85$ for $L/D \geq 14.0$. At farther downstream locations, a sharp decrease of the pressure fluctuations can be seen and the presence of the cavity results in higher levels of pressure fluctuations except for the case of transitional-type cavity ($L/D = 11.7$). The peak pressure fluctuations followed by a sharp decrease indicate that the intermittent nature of the flow is a localized phenomenon of the shock wave excursion, which is shown by the raw pressure signals.

The peak pressure fluctuations suggest the intermittency of the cavity-convex corner interaction and can be used as an indication of flow unsteadiness. For the convex-corner flow (Fig. 9a), the amplitude of peak pressure fluctuations increases with $M_\infty^2\eta$. The intense pressure fluctuations are associated with the initial compression and excursion of the shock wave downstream of the corner. With the upstream cavity at $Z^* = 1$, the data of peak pressure fluctuations $C_{\sigma_p,\max}$ for all of the test cases are summarized in Fig. 9a. It is found that the open- or transitional-type cavities result in a slight increase of $C_{\sigma_p,\max}$ for the subsonic convex-corner flows ($M_\infty^2\eta = 5.32$). Slight damping is observed with the closed-type cavities ($L/D = 21.0$ and 35.0). For the attached transonic flows ($M_\infty^2\eta = 6.14$ and 6.96), the cavities result in the increase of $C_{\sigma_p,\max}$. This may be due to the superposition of flow unsteadiness induced by the initial compression and the downstream propagation of the disturbance by the upstream cavity. At $M_\infty^2\eta = 8.96$, the oil-flow visualization indicates the delay of boundary-layer separation with the open- or transitional-type cavities, in which the decrease of $C_{\sigma_p,\max}$, is observed. For the separated flows ($M_\infty^2\eta = 10.33$ and 11.71), the peak interaction occurs at the location of flow separation. The upstream cavity has a strong influence on the intensity of pressure fluctuations. Higher levels of pressure oscillation are due to the intense shock wave excursion except for the case with the transitional-type cavity ($L/D = 11.7$). The data are replotted in Fig. 9b to help understand the geometric effect of the cavity. It can be seen that the levels of $C_{\sigma_p,\max}$ are related to the minimum static pressure for the attached flows. Larger $C_{\sigma_p,\max}$ values are associated with decreasing $C_{p,\min}$ (or higher initial pressure rise). For $M_\infty^2\eta = 10.33$ and 11.71, the oil-flow visualization indicates that the separation location moves downstream with the transitional-type cavity and propagates upstream with the open- or closed-type cavities. This results in the variation of peak pressure fluctuations with L/D. When the cavities move upstream ($Z^* = 2$), the variations of $C_{\sigma_p,\max}$ with $M_\infty^2\eta$ or L/D show the similar trend as those at $Z^* = 1$. Higher intensity of $C_{\sigma_p,\max}$ are observed with increasing $M_\infty^2\eta$ except for the case at $M_\infty^2\eta = 8.96$ (Fig. 10a). For a given $M_\infty^2\eta$ (Fig. 10b), the L/D effect is less significant, particularly with the transitional-type cavity. At $Z^* = 3$, it appears that the amplitude of $C_{\sigma_p,\max}$ is roughly the same as $L/D = 7.0$ at $Z^* = 2$. The influence of Z^* can be seen at $L/D = 2.0$, in which $C_{\sigma_p,\max}$ is smaller at $Z^* = 3$.

Conclusions

The present study investigates cavity-convex corner interactions. The geometric effects of the cavity, spacing distance, Mach number, and the convex-corner angle are shown to be as follows.

1) The upstream cavity induces stronger upstream expansion and downstream initial compression for the subsonic expansion flows. Delay of the transition of subsonic and transonic expansion flows is also observed. Higher levels of downstream pressure fluctuations

are associated with the open- and transitional-type cavities for the attached flows.

2) The spacing has a significant effect on the delay of the initial boundary-layer separation.

3) For the separated flows with open- or closed-type cavities, the shock location moves upstream, and the reattachment expands slight downstream. The cavity effect is limited near the convex corner. The influence of transitional-type cavity is minimized.

4) Higher static pressure downstream of the corner is associated with the upstream movement of shock wave, particularly with the closed-type cavity.

5) The peak interactions occur downstream of the corner and are associated with the initial pressure rise and shock wave excursion. For separated flows, the intermittency (or peak pressure fluctuation) is a localized phenomenon.

6) Open- or closed-type cavities enhance the unsteadiness of the convex-corner flows.

Acknowledgments

This research was carried out with the support of the National Science Council (NSC 89-2612-E-006-019). The author also thanks the technical assistance of Aerospace Science and Technology Research Center/National Cheng Kung University technical staffs.

References

[1]Bolonki, A., and Gilyard, G. B., "Estimated Benefits of Variable-Geometry Wing Camber Control for Transport Aircraft," NASA TM-1999-206586, Oct. 1999.

[2]Chung, K. M., "Investigation on Transonic Convex-Corner Flows," *Journal of Aircraft*, Vol. 39, No. 6, 2002, pp. 1014–1018.

[3]Chung, K. M., "Pressure Fluctuations in Rectangular Cavity Flows," *The Chinese Journal of Mechanics*, Vol. 15, No. 3, 1999, pp. 97–102.

[4]Zhang, X., "Compressible Cavity Flow Oscillation due to Shear Layer Instabilities and Pressure Feedback," *AIAA Journal*, Vol. 33, No. 8, 1995, pp. 1404–1411.

[5]Corcos, G. M., "Resolution of Pressure in Turbulence," *Journal of the Acoustical Society of America*, Vol. 35, No. 2, 1963, pp. 192–199.

[6]Miau, J., Cheng, J., Chung, K., and Chou, J., "The Effect of Surface Roughness on the Boundary Layer Transition," *Proceeding 7th International Symposium in Flow Modeling and Turbulent Measurement*, International Association for Hydraulic Research, National Cheng Kung University, Tainan, Taiwan, 1998, pp. 609–616.